Eur. Phys. J. D **13**, 401–413 (2001)

THE EUROPEAN PHYSICAL JOURNAL D

EDP Sciences

Spectral linewidth of inversionless and Raman lasers in V-type three-level systems

X.-m. Hu[a], J. Xiong, and J.-s. Peng

Department of Physics, Huazhong Normal University, Wuhan 430079, P.R. China

Received 25 October 1999 and Received in final form 10 March 2000

Abstract. A theoretical analysis of the spectral linewidth of V-type inversionless and Raman lasers is presented. First, we examine the effects of the atomic coherence between dressed states and the Autler-Townes splitting on the linewidth. It is demonstrated that near above threshold, the V inversionless laser has a narrower linewidth than that of the two-level laser. Instead of the dressed coherence, it is the Autler-Townes splitting that is responsible for the linewidth reduction though the dressed coherence determines the laser gain. Next, we explore the effects of the generated laser intensity on the linewidth. It is shown that the linewidths of the V inversionless and Raman lasers follow the usual $1/I$ decrease for smaller laser intensity I, but a slower decrease than $1/I$ for larger laser intensity. For the V Raman laser, even more surprisingly, with the laser intensity increasing, the linewidth appreciably increases as well. As a result, well above threshold, the V inversionless and Raman lasers may have a larger linewidth than that of the two-level laser. Finally, a comparison is made between the V lasers and the Λ lasers. It is found that the linewidth of the Λ inversionless laser shows a fast $1/I^2$ decay under optimum conditions.

PACS. 42.50.Lc Quantum fluctuations, quantum noise, and quantum jumps – 42.50.Gy Effects of atomic coherence on propagation, absorption, and amplification of light

1 Introduction

The spectral linewidth of a two-level laser (TLL) is given by the known Schawlow-Townes formula [1–4]

$$D_{\phi\phi}^{\mathrm{TLL}} = \frac{A}{2\bar{n}}, \tag{1}$$

where A is the linear gain coefficient and gives the rate of increase in the mean number of photons due to spontaneous emission, and $\bar{n}$ is the mean number of photons in the cavity. It is well-known that the gain A arises from population inversion.

Recently much attention has been paid to quantum statistical properties [5–14] of driven multilevel systems, in particular, those that generate lasers without inversion [15–25]. Agarwal [5] showed that for weak laser fields, a laser without inversion may have a narrower linewidth than that of TLL. In terms of the linear analysis [5,6], the linewidth of the Λ inversionless laser is expressed as

$$D_{\phi\phi}^{\Lambda} = \frac{A}{2\bar{n}} f, \tag{2}$$

where $S = Af$ describes the rate of increase of the mean number of photons due to spontaneous emission. Formula (2) differs from (1) in two aspects. First, the gain A in formula (2) originates not from population inversion but from atomic coherence. Compared with TLL, the inversionless gain is usually very small. In particular, in the strong driving limit, *i.e.*, $I_0 \gg \gamma_i\gamma_j$ where γ's are the atomic decay rates and I_0 is the driving field intensity, one has the inversionless gain $A \sim O(\gamma_i\gamma_j/I_0)$ [17–19]. Secondly, in formula (2), the deviation factor $f = f(\Lambda_i, \gamma_j, I_0) \neq 1$. This depends on the incoherent pumping rates Λ_i, the decay rates γ_j, and the driving field intensity I_0. Even in the adiabatic limit [6], the deviation factor is smaller than 1, *i.e.*, $f < 1$. For the above two differences, the Λ inversionless laser has a linewidth far below that of TLL, *i.e.*,

$$D_{\phi\phi}^{\Lambda} \ll D_{\phi\phi}^{\mathrm{TLL}}, \tag{3}$$

if the mean photon numbers are equal for both cases.

To our knowledge, until now, no description showing the physical cause of linewidth narrowing has been reported. Most often, one employs dressed states to analyze the physical origin of the inversionless amplification. It has been identified that two different mechanisms are responsible for the inversionless gain. The first is connected

[a] e-mail: xmhu@phy.ccnu.edu.cn

with the appearance of a population inversion between atomic states dressed by the coherent pump, while the second is linked to the buildup of coherence among these states [18,19]. The inversionless gain has been demonstrated [20–23] experimentally and the first lasers without inversion have been realized [24,25]. For the inversionless laser based on the dressed coherence [17–19], it seems as if the dressed coherence was responsible for linewidth narrowing. On the other hand, the spontaneous emission of a driven three-level atom is a two-peak distribution due to the Autler-Townes splitting [26–28]. Recently, it has been shown that even a dark line can appear in the spectrum of a driven Λ atom under the ideal conditions [29]. Also, one could expect that the Autler-Townes splitting plays an important role in the linewidth reduction. As will be shown later, it is not the dressed coherence but the Autler-Townes splitting that results in the linewidth narrowing.

Near above threshold, the linear analysis is sufficient for the description of the laser linewidth. Well above threshold, however, the complete analysis requires to solve the self-consistent equation for the laser field. For TLL, as is well known, the linewidth still follows the $1/I$ decay when the saturation effect of the laser intensity $I = g^2\bar{n}$ is taken into account [2–4]. However, the linewidths of the driven multilevel systems can have different features. Ritsch *et al.* [7] has shown that for the weak coherent driving, the linewidth of the Λ Raman laser displays a fast $1/I^3$ decay. For the Λ inversionless laser, however, the dependence of the linewidth on the laser intensity has not yet given so far. As a by-product of this paper, we will show that the linewidth of the Λ inversionless laser decreases with $1/I^2$.

So far, most work on quantum statistical properties in driven systems has mainly been confined to Λ systems [5–14]. Although the V and Λ systems have many similar properties, there exist distinct differences between them. In the V system the coherence has lifetime even shorter than the lifetime of the laser transition while the Λ system may have long living coherence. Unlike the Λ system that generates intensity-squeezed light, the intensity fluctuation of V inversionless laser is above the shot-noise limit [14]. Up to now, however, no discussion has been reported on the linewidth of V inversionless and Raman lasers.

This paper is devoted to investigate the linewidths of the V inversionless and Raman lasers. We first analyze the roles of the dressed coherence and the Autler-Townes splitting, then discuss the effects of the laser intensity, and finally make a comparison between the V lasers and the Λ lasers.

2 Model and master equation

We will now employ a unified model to describe both an inversionless laser and a Raman laser. The model consists of N three-level atoms in the V configuration interacting with a quantum mechanical cavity mode and a classical external field. The laser transition is the $|1\rangle-|2\rangle$ transition and the external field is applied on the $|2\rangle-|3\rangle$ transition. The atoms decay spontaneously from the excited states $|1\rangle$ and $|3\rangle$ to ground state $|2\rangle$ with the rates $2\bar{\gamma}_1$ and $2\gamma_2$, respectively. If an incoherent pump between $|1\rangle$ and $|2\rangle$ with a rate 2Λ is used, the present model is identical to the scheme of a laser without inversion, studied by Zhu *et al.* [14,18]. If a spontaneous decay from $|3\rangle$ to $|1\rangle$ with a rate $2\gamma_3$ is substituted for the incoherent pump, the model is the Raman scheme. That is to say, the present model serves as the inversionless laser for $\Lambda \neq 0$ and $\gamma_3 = 0$, and as the Raman laser for $\Lambda = 0$ and $\gamma_3 \neq 0$. From now on, this definition will be used without further specializations. In the rotating wave and dipole approximations, the system Hamiltonian can be written as

$$H = \Delta_c a^\dagger a + \sum_{j=1}^{N}[\Delta_1\sigma_{11}^j + \Delta_2\sigma_{33}^j + g(a^\dagger\sigma_{21}^j + \sigma_{12}^j a) + \Omega_0(\sigma_{23}^j + \sigma_{32}^j)]. \quad (4)$$

The operators $a^\dagger$ and a are, respectively, the creation and annihilation operators of the cavity field, and $\sigma_{lk}^j = |l^j\rangle\langle k^j|$ denotes the population operator of jth atom for $l = k$ and the polarization operator for $l \neq k$. Ω_0 labels the real-valued Rabi frequency of the driving field, and g is the coupling strength of the atoms and the cavity field. $\Delta_1 = \omega_{12} - \omega_1$ ($\Delta_2 = \omega_{32} - \omega_2$) denotes the detuning on the laser (pump) transition, and $\Delta_c = \omega_c - \omega_1$ describes the cavity detuning. In the expressions of Δ_i ($i = 1, 2, c$), ω_{12} (ω_{32}) is the frequency of the transition $|1\rangle-|2\rangle$ ($|2\rangle-|3\rangle$), ω_1 (ω_2) is the frequency of the cavity (driving) field, and ω_c is the frequency of the empty cavity. The master equation of the system takes the form

$$\dot{\rho} = -i[H,\rho] + \frac{1}{2}\kappa\mathcal{L}_c\rho + \sum_{j=1}^{N}(\Lambda\mathcal{L}_{21}^j\rho + \gamma_1\mathcal{L}_{12}^j\rho + \gamma_2\mathcal{L}_{32}^j\rho + \gamma_3\mathcal{L}_{31}^j\rho), \quad (5)$$

where $\gamma_1 = \bar{\gamma}_1 + \Lambda$ and κ is the cavity loss rate. The relaxation terms read

$$\begin{aligned}
\mathcal{L}_c^j\rho &= 2a\rho a^\dagger - aa^\dagger\rho - \rho aa^\dagger,\\
\mathcal{L}_{21}^j\rho &= 2\sigma_{12}^j\rho\sigma_{21}^j - \sigma_{21}^j\sigma_{12}^j\rho - \rho\sigma_{21}^j\sigma_{12}^j,\\
\mathcal{L}_{12}^j\rho &= 2\sigma_{21}^j\rho\sigma_{12}^j - \sigma_{12}^j\sigma_{21}^j\rho - \rho\sigma_{12}^j\sigma_{21}^j,\\
\mathcal{L}_{32}^j\rho &= 2\sigma_{23}^j\rho\sigma_{32}^j - \sigma_{32}^j\sigma_{23}^j\rho - \rho\sigma_{32}^j\sigma_{23}^j,\\
\mathcal{L}_{31}^j\rho &= 2\sigma_{13}^j\rho\sigma_{31}^j - \sigma_{31}^j\sigma_{13}^j\rho - \rho\sigma_{31}^j\sigma_{13}^j.
\end{aligned} \quad (6)$$

In the subsequent sections, we will present a detailed analysis of the spectral linewidths of the V inversionless and Raman lasers.

3 Linear analysis in dressed state picture

3.1 Langevin equations

In order to examine the effects of the atomic coherence and the Autler-Townes splitting on the linewidth, we employ the dressed state basis and the linear perturbation

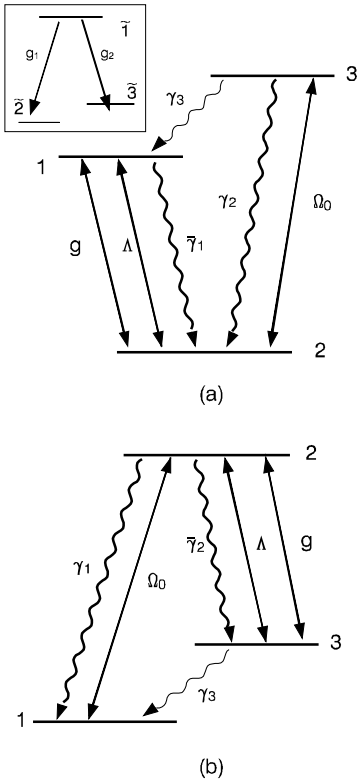

Fig. 1. (a) Schematic representation of V systems. The inset denotes the corresponding representation in the dressed state basis. (b) Schematic representation of Λ systems.

method. The dressed states, which are the eigenstates of $V^j = \Delta_2\sigma_{33}^j + \Omega_0(\sigma_{23}^j + \sigma_{32}^j)$, are written as:

$$\begin{aligned} |\tilde{1}^j\rangle &= |1^j\rangle, \\ |\tilde{2}^j\rangle &= \cos\theta|2^j\rangle + \sin\theta|3^j\rangle, \\ |\tilde{3}^j\rangle &= \sin\theta|2^j\rangle - \cos\theta|3^j\rangle, \end{aligned} \tag{7}$$

where $\tan(2\theta) = 1/\delta$, $\delta = \Delta_2/(2\Omega_0)$ and $0 \le \theta \le \pi/2$. The dressed states $|\tilde{2}^j\rangle$ and $|\tilde{3}^j\rangle$ (*i.e.*, the Autler-Townes doublet, shown in the inset of Fig. 1a) have corresponding eigenvalues $\lambda_{2,3} = (\Delta_2 \mp \Omega)/2$, where $\Omega = (\Delta_2^2 + 4\Omega_0^2)^{1/2}$ describes the gap between the dressed states. In the dressed state basis, the atomic variables are written as $\tilde{\sigma}_{lk}^{\mu} = |\tilde{l}^{\mu}\rangle\langle\tilde{k}^{\mu}|$.

The equivalent form of master equation (5) in the dressed state basis is derived in Appendix A. Since we consider a large number of independent atoms we can describe the system using collective variables $\tilde{\sigma}_{lk} = (1/N)\sum_{j=1}^{N}\tilde{\sigma}_{lk}^j$. In order to determine the statistical properties of the laser field, we apply a c-number Langevin approach [2–4]. The operator master equation (A.2) is equivalent to a c-number Fokker-Planck equation for the generalized P representation of Drummond and Gardiner [30]. Here we choose the normal ordering $a^\dagger$, $\tilde{\sigma}_{12}$, $\tilde{\sigma}_{13}$, $\tilde{\sigma}_{23}$, $\tilde{\sigma}_{11}$, $\tilde{\sigma}_{22}$, $\tilde{\sigma}_{33}$, $\tilde{\sigma}_{32}$, $\tilde{\sigma}_{31}$, $\tilde{\sigma}_{21}$, a and define a correspondence between c numbers and operators as $\alpha^\dagger \leftrightarrow a^\dagger$, $R_{ij} \leftrightarrow \tilde{\sigma}_{ij}$, $\alpha \leftrightarrow a$. From the equation (A.2) in Appendix A, we can easily derived the Langevin equations,

$$\begin{aligned} \dot{\alpha} &= -(\kappa/2 + \mathrm{i}\Delta_c)\alpha - \mathrm{i}g_1 N R_{21} - \mathrm{i}g_2 N R_{31} + F_\alpha(t), \\ \dot{R}_{11} &= -2\gamma_1 R_{11} + 2\Lambda_1 R_{22} + 2\Lambda_2 R_{33} + 2\Lambda_c(R_{23} + R_{32}) \\ &\quad + \mathrm{i}g_1(\alpha^\dagger R_{21} - R_{12}\alpha) \\ &\quad + \mathrm{i}g_2(\alpha^\dagger R_{31} - R_{13}\alpha) + F_{R_{11}}(t), \\ \dot{R}_{22} &= 2\Gamma_1 R_{11} - 2(\Lambda_1 + \Gamma_{23})R_{22} + 2\Gamma_{32}R_{33} \\ &\quad - (\Lambda_c + \Gamma_c)(R_{23} + R_{32}) \\ &\quad - \mathrm{i}g_1(\alpha^\dagger R_{21} - R_{12}\alpha) + F_{R_{22}}(t), \\ \dot{R}_{33} &= 2\Gamma_2 R_{11} + 2\Gamma_{23}R_{22} - 2(\Lambda_2 + \Gamma_{32})R_{33} \\ &\quad - (\Lambda_c - \Gamma_c)(R_{23} + R_{32}) \\ &\quad - \mathrm{i}g_2(\alpha^\dagger R_{31} - R_{13}\alpha) + F_{R_{33}}(t), \\ \dot{R}_{21} &= -(\tilde{\gamma}_{21} + \mathrm{i}\tilde{\Delta}_1)R_{21} + (\gamma_c - \Lambda_c)R_{31} + \mathrm{i}g_1\alpha(R_{11} - R_{22}) \\ &\quad - \mathrm{i}g_2\alpha R_{23} + F_{R_{21}}(t), \\ \dot{R}_{31} &= -(\tilde{\gamma}_{31} + \mathrm{i}\tilde{\Delta}_2)R_{31} + (\gamma_c - \Lambda_c)R_{21} + \mathrm{i}g_2\alpha(R_{11} - R_{33}) \\ &\quad - \mathrm{i}g_1\alpha R_{32} + F_{R_{31}}(t), \\ \dot{R}_{32} &= -(\tilde{\gamma}_{32} + \mathrm{i}\tilde{\Delta}_3)R_{32} + 2\Gamma_q R_{11} + (2\gamma_c - \Lambda_c)(R_{22} + R_{33}) \\ &\quad - \Gamma_c(R_{22} - R_{33}) - 2\Gamma_p R_{23} + \mathrm{i}g_2\alpha R_{12} \\ &\quad - \mathrm{i}g_1\alpha^\dagger R_{31} + F_{R_{32}}(t), \end{aligned} \tag{8}$$

where the parameters are presented in Appendix B. The closure of the system requires $R_{11} + R_{22} + R_{33} = 1$. The noise correlations are generally written as

$$\langle F_x(t)F_y(t')\rangle = (2/N)\langle D_{xy}\rangle\delta(t - t'), \qquad (x, y = \alpha, \alpha^\dagger, R_{ij}). \tag{9}$$

In the lowest order of the laser field the only relevant noise contributions, however, come from $F_{R_{21}}$ and $F_{R_{32}}$:

$$\begin{aligned} 2\langle D_{R_{12}R_{21}}\rangle &= 2[(\Lambda_1 + \Gamma_{23} + \Gamma_p)R_{11} \\ &\quad + \Lambda_1 R_{22} + \Lambda_2 R_{33} + \Lambda_c(R_{23} + R_{32})], \\ 2\langle D_{R_{13}R_{31}}\rangle &= 2\langle D_{R_{12}R_{21}}\rangle, \\ 2\langle D_{R_{12}R_{31}}\rangle &= 2(\Lambda_c - \gamma_c)R_{11}. \end{aligned} \tag{10}$$

In what follows, the comparison between the two special cases will be made. One is that the laser frequency lies symmetrically between the Autler-Townes peaks (*i.e.*, $\tilde{\Delta}_1 = -\tilde{\Delta}_2 = \Omega_0$) and the other is that the laser frequency is consistent with either of the Autler-Townes peaks (*i.e.*, $\tilde{\Delta}_1 = 0$ or $\tilde{\Delta}_2 = 0$).

3.2 Linewidth for $\tilde{\Delta}_1 = -\tilde{\Delta}_2 = \Omega_0$

In the case of $\tilde{\Delta}_1 = -\tilde{\Delta}_2 = \Omega_0$, we have $g_1 = g_2$, $\Lambda_1 = \Lambda_2$, $\Gamma_1 = \Gamma_2$ and $\Gamma_{23} = \Gamma_{32}$. As usual, it is assumed that the atomic variables are eliminated adiabatically under the assumption $\gamma_i, \gamma_{ij} \gg \kappa$. Furthermore, we consider zero cavity detuning (*i.e.*, $\Delta_c = 0$) without the loss of generality. Using the perturbation method, we can obtain from equation (8) the linear Langevin equation for the laser

field α

$$\dot{\alpha} = \frac{1}{2}(A-\kappa)\alpha + F(t), \tag{11}$$

where A is the linear gain,

$$\begin{aligned} A &= A_{\rm p} + A_{\rm c}, \\ A_{\rm p} &= g^2 N(\gamma_1+\gamma_2)(2R_{11}-R_{22}-R_{33})/D_1, \\ A_{\rm c} &= g^2 N[-(\gamma_1+\gamma_2+{\rm i}\Omega_0)R_{23}-(\gamma_1+\gamma_2-{\rm i}\Omega_0)R_{32}]/D_1, \end{aligned} \tag{12}$$

and F is the noise force,

$$\begin{aligned} F(t) = F_\alpha(t) &- \frac{{\rm i}g(\gamma_1+\gamma_2-{\rm i}\Omega_0)}{\sqrt{2}D_1}F_{R_{21}}(t) \\ &- \frac{{\rm i}g(\gamma_1+\gamma_2+{\rm i}\Omega_0)}{\sqrt{2}D_1}F_{R_{31}}(t), \end{aligned} \tag{13}$$

with $D_1 = \Omega_0^2 + (\gamma_1+\gamma_2)(\gamma_1+\Lambda)$.

In equation (12), $A_{\rm p}$ is the population contribution while $A_{\rm c}$ denotes the coherence contribution. Under the noninversion condition ($R_{11} < R_{22}, R_{33}$), the population contribution is negative, *i.e.*, $A_{\rm p} < 0$. Only when the coherence contribution exceeds the population contribution (*i.e.*, $A_{\rm c} > |A_{\rm p}|$) can the laser action be initiated. In the present linear theory, the population R_{ii} and the coherence R_{23} have the zeroth-order solutions

$$\begin{aligned} R_{11} &= \Lambda[I_0 + \gamma_2(\gamma_2+\Lambda)]/D_2, \\ R_{22} &= R_{33} = \gamma_1[I_0 + \gamma_2(\gamma_2+\Lambda)/2]/D_2, \\ R_{23} &= \gamma_1\gamma_2[(\gamma_2+\Lambda)/2 + {\rm i}\Omega_0]/D_2, \end{aligned} \tag{14}$$

where $I_0 = \Omega_0^2$ and $D_2 = (2\gamma_1+\Lambda)I_0 + \gamma_2(\gamma_1+\Lambda)(\gamma_2+\Lambda)$. The threshold conditions can easily be obtained from $A > 0$ and $R_{11} < R_{22}, R_{33}$. For any small cavity loss rate κ, the simple analytical expression for the threshold value of the driving field Rabi frequency can be obtained,

$$\Omega_0 > \max\left[\left(\frac{(\gamma_1-2\Lambda)\gamma_2\gamma_{13}}{2(\gamma_1-\Lambda)}\right)^{1/2}, \left(\frac{(\gamma_1-\Lambda)\gamma_2\gamma_{13}\gamma_{23}}{\gamma_1\gamma_2-(\gamma_1-\Lambda)\gamma_{13}}\right)^{1/2}\right], \tag{15}$$

which shows that the minimum value of the required Rabi frequency is of at least the same order as the atomic decay rates. For given cavity loss rate κ, as will be seen from equation (27), the required driving field Rabi frequency has its upper limit $\Omega_0^{\max}$. In order to show the effect of the Autler-Townes splitting, we assume that the Autler-Townes peaks are well separated. It is the case when the driving field is strong enough, *i.e.*, $\Omega_0 \gg \gamma_j$. Taking into account the above two factors, by "the strong driving limit" we mean $\gamma_j \ll \Omega_0 < \Omega_0^{\max}$ through this paper.

In the strong driving limit, this system operates without population inversion when the rate of incoherent pumping satisfies $\Lambda < \gamma_1$. Then the gain takes the simple form

$$A = \frac{g^2 N(\Lambda\gamma_1 + \Lambda\gamma_2 - \gamma_1^2)}{I_0(\Lambda+2\gamma_1)}. \tag{16}$$

The positive gain requires $\gamma_1 > \Lambda > \gamma_1^2/(\gamma_1+\gamma_2)$, which implies that the decay rate on the driving transition should be bigger than the decay rate on the laser transition, *i.e.*, $\gamma_2 > \gamma_1$.

Following the standard technique [2–4], we get the laser linewidth

$$\begin{aligned} D_{\phi\phi} &= D_{\phi\phi}^{\rm p} + D_{\phi\phi}^{\rm c}, \\ D_{\phi\phi}^{\rm p} &= \frac{g^2 N}{2\bar{n}D_1^2}\{2[\Lambda(\gamma_1+\gamma_2)^2 + \gamma_2 I_0]R_{11} \\ &\quad + \Lambda[(\gamma_1+\gamma_2)^2 + I_0](R_{22}+R_{33})\}, \\ D_{\phi\phi}^{\rm c} &= \frac{g^2 N}{2\bar{n}D_1^2}\{\Lambda[(\gamma_1+\gamma_2)^2 + I_0](R_{23}+R_{32})\}, \end{aligned} \tag{17}$$

where $\bar{n} = \alpha^\dagger\alpha$ is the mean photon number in the cavity. In equation (17), $D_{\phi\phi}^{\rm p}$ is linked to the populations R_{ii} (i = 1–3) while $D_{\phi\phi}^{\rm c}$ is connected with the dressed coherence R_{23}. In the strong driving limit, they reduce to

$$\begin{aligned} D_{\phi\phi}^{\rm p} &= \frac{g^2 N}{2\bar{n}}\left[\frac{2\Lambda(\gamma_1+\gamma_2)}{I_0(\Lambda+2\gamma_1)}\right], \\ D_{\phi\phi}^{\rm c} &= \frac{g^2 N}{2\bar{n}}\left[\frac{\gamma_1\gamma_2\Lambda(\gamma_2+\Lambda)}{I_0^2(\Lambda+2\gamma_1)}\right], \end{aligned} \tag{18}$$

and have the relation $D_{\phi\phi}^{\rm c}/D_{\phi\phi}^{\rm p} \sim O(\gamma_i\gamma_j/I_0)$. Obviously, the total linewidth, which is mainly determined by $D_{\phi\phi}^{\rm p}$, satisfies

$$D_{\phi\phi} \ll D_{\phi\phi}^{\rm TLL}, \tag{19}$$

if the mean photon numbers are equal for the two cases. The relations (3, 19) show that not only the Λ inversionless laser but also the V inversionless laser has a much narrower linewidth than that of TLL.

3.3 Linewidth for $\tilde{\Delta}_1 = 0$

For the general detunings $\tilde{\Delta}_1$ and $\tilde{\Delta}_2$, the linear gain is calculated as

$$\begin{aligned} A &= A_{\rm p} + A_{\rm c}, \\ A_{\rm p} &= 2g^2 N[a_1(R_{11}-R_{22}) + a_2(R_{11}-R_{33})], \\ A_{\rm c} &= 2g^2 N\,{\rm Re}(b_1 R_{23} + b_2 R_{32}), \end{aligned} \tag{20}$$

where the populations R_{ii} (i = 1–3), the dressed coherence R_{23} and the parameters a_i, b_i (i = 1, 2) are given in Appendix C.

Let's now focus on the case of the resonance on the transition $|\tilde{1}^j\rangle - |\tilde{2}^j\rangle$, *i.e.*, $\tilde{\Delta}_1 = 0$ together with $\tilde{\Delta}_2 = \tilde{\Delta}_3 = -2\Omega_0$. In the strong driving limit where we have $a_1 \gg a_2, b_2, b_3$, and $R_{11}, R_{22}, R_{33} \gg {\rm Re}(R_{23}), {\rm Im}(R_{23})$, the gain is simplified as $A \approx 2g^2 N a_1(R_{11}-R_{22})$, which shows that one needs population inversion between the dressed states $|\tilde{1}^j\rangle$ and $|\tilde{2}^j\rangle$ to facilitate gain. The inversion can be achieved by properly adjusting the detuning

Δ_2, and keeping the other parameters the same as in the above subsection. The laser linewidth has the form

$$\begin{aligned} D_{\phi\phi} &= D^{\rm p}_{\phi\phi} + D^{\rm c}_{\phi\phi}, \\ D^{\rm p}_{\phi\phi} &= \frac{g^2 N}{2\bar{n}} \left\{ \begin{array}{l} c_1[(\Lambda_1 + \Gamma_{23} + \Gamma_{\rm p})R_{11} \\ +\Lambda_1 R_{22} + \Lambda_2 R_{33}] \\ +c_2[(\Lambda_2 + \Gamma_{32} + \Gamma_{\rm p})R_{11} \\ +\Lambda_1 R_{22} + \Lambda_2 R_{33}] \\ +c_3(\Lambda_{\rm c} - \gamma_{\rm c})R_{11} \end{array} \right\}, \qquad (21) \\ D^{\rm c}_{\phi\phi} &= \frac{g^2 N}{2\bar{n}}[(c_1 + c_2)\Lambda_{\rm c}(R_{23} + R_{32})], \end{aligned}$$

where the parameters c_i ($i = 1$–3) are listed in Appendix D. In the expression of $D^{\rm p}_{\phi\phi}$, the term proportional to c_1 (c_2) comes from spontaneous emission on the $|\tilde{1}^j\rangle$–$|\tilde{2}^j\rangle$ ($|\tilde{1}^j\rangle$–$|\tilde{3}^j\rangle$) transition, while the term containing c_3 is due to the coupling between the polarizations R_{21} and R_{31}. In the strong driving limit, we have $D^{\rm p}_{\phi\phi} \gg D^{\rm c}_{\phi\phi}$, which shows that the atomic coherence plays a negligible role. The linewidth $D_{\phi\phi}$ depends mainly on the population contribution $D^{\rm p}_{\phi\phi}$. Then we obtain

$$\begin{aligned} D_{\phi\phi} &\approx \frac{g^2 N}{2\bar{n}} c_1[(\Lambda_1 + \Gamma_{23} + \Gamma_p)R_{11} + \Lambda_1 R_{22} + \Lambda_2 R_{33}] \\ &\sim \frac{g^2 N}{2\bar{n}\gamma_{21}} \sim D^{\rm TLL}_{\phi\phi}, \qquad (22) \end{aligned}$$

which shows that the linewidth for $\tilde{\Delta}_1 = 0$ is far above the linewidth for $\tilde{\Delta}_1 = -\tilde{\Delta}_2 = \Omega_0$ if the mean photon numbers are equal for these two cases.

3.4 Discussion

In the above two subsections it has been shown that the dressed coherence plays a negligible small role in the linewidth reduction. What causes the linewidth reduction? In the dressed state basis (see the inset in Fig. 1a), the spontaneous emission occurs from the excited state $|\tilde{1}\rangle$ to the Autler-Townes doublet states $|\tilde{2}\rangle$ and $|\tilde{3}\rangle$. When $\tilde{\Delta}_1 = -\tilde{\Delta}_2 = \Omega_0$, two peaks of spontaneous emission spectrum center at $\omega_{12} \pm \Omega_0$, respectively. In this case, the laser frequency locates symmetrically between the two peaks. In the strong driving limit, the two peaks are far away from the laser frequency. It is easily understood that the linewidth of the V inversionless laser is far below that of TLL, *i.e.*, $D_{\phi\phi}/D^{\rm TLL}_{\phi\phi} \sim O(\gamma_i\gamma_j/I_0)$. In the case of $\tilde{\Delta}_1 = 0$, however, the laser frequency coincides with one of spontaneous spectrum peaks. Thus the spontaneous emission has a strong effect on the phase diffusion and the linewidth is greatly increased, $D_{\phi\phi}/D^{\rm TLL}_{\phi\phi} \sim 1$. The comparison between the two cases clearly reveals that Aulter-Townes splitting is responsible for linewidth narrowing.

So far, we have shown that near above threshold, the V inversionless laser may have a much narrower linewidth than that of TLL, and that the linewidth narrowing results from the Aulter-Townes splitting instead of the dressed coherence. We would like to point out that these results hold for the inversionless lasers in Λ and cascade configurations. It should be noted that the absence of inversion is not necessary to have a narrow linewidth. In fact, it is easy to show from equations (12, 13, 17) that even under population inversion, the linewidth of the V driven system may be much narrower than that of TLL. This problem will be mentioned later. The above linear analysis is only valid near above threshold. Well above threshold, we have to resort to the nonlinear analysis which requires the solution to the self-consistent equation for the laser field.

4 Nonlinear analysis in bare state picture

In this section, we discuss the saturation effects of the generated laser intensity. For this purpose, it is most convenient to work in the bare state basis. We use the collective atomic operator $\sigma_{lk} = (1/N)\sum_{j=1}^{N}\sigma^j_{lk}$ and choose the normal ordering $a^\dagger$, σ_{12}, σ_{32}, σ_{13}, σ_{11}, σ_{22}, σ_{33}, σ_{31}, σ_{23}, σ_{21}, a. Furthermore, we define the correspondence between c numbers and operators as $\alpha^\dagger \leftrightarrow a^\dagger$, $v_{12} \leftrightarrow -{\rm i}\sigma_{12}$, $v_{23} \leftrightarrow -{\rm i}\sigma_{23}$, $v_{13} \leftrightarrow \sigma_{13}$, $v_{21} \leftrightarrow {\rm i}\sigma_{21}$, $v_{32} \leftrightarrow {\rm i}\sigma_{32}$, $v_{31} \leftrightarrow \sigma_{31}$, $\alpha \leftrightarrow a$. The set of c-number Langevin equations are derived from the master equation (5) as

$$\begin{aligned} \dot{\alpha} &= -(\kappa/2 + {\rm i}\Delta_{\rm c}) + gNv_{21} + F_\alpha, \\ \dot{v}_{12} &= -(\gamma_{12} - {\rm i}\Delta_1)v_{12} + g\alpha^\dagger(v_{11} - v_{22}) \\ &\quad +\Omega_0 v_{13} + F_{v_{12}}, \\ \dot{v}_{23} &= -(\gamma_{23} + {\rm i}\Delta_2)v_{23} + \Omega_0(v_{33} - v_{22}) + g\alpha v_{13} + F_{v_{23}}, \\ \dot{v}_{13} &= -[(\gamma_{13} + {\rm i}(\Delta_2 - \Delta_1)]v_{13} - gv_{23} \\ &\quad -\Omega_0 v_{12} + F_{v_{13}}, \\ \dot{v}_{11} &= -2\gamma_1 v_{11} + 2\Lambda v_{22} + 2\gamma_3 v_{33} - g\alpha^\dagger v_{21} \\ &\quad -g\alpha v_{12} + F_{v_{11}}, \\ \dot{v}_{33} &= -2(\gamma_2 + \gamma_3)v_{33} - \Omega_0 v_{23} - \Omega_0 v_{32} + F_{v_{33}}, \qquad (23) \end{aligned}$$

where $\gamma_{12} = \Lambda + \gamma_1$, $\gamma_{23} = \Lambda + \gamma_2 + \gamma_3$, $\gamma_{13} = \gamma_1 + \gamma_2 + \gamma_3$. The population v_{22} is solved by the closure relation $v_{11} + v_{22} + v_{33} = 1$. The nonzero diffusion coefficients associated with the linewidth are given in Appendix E.

We consider the resonant case (*i.e.*, $\Delta_1 = \Delta_2 = \Delta_{\rm c} = 0$), which is identical to the case of Section 3.2. After adiabatically eliminating the atomic variables, we obtain from equations (23) the Langevin equation for the laser field α,

$$\dot{\alpha} = \frac{1}{2}(G - \kappa)\alpha + F(t), \qquad (24)$$

where $G = G(I)$ and F are the nonlinear gain and the Langevin force respectively,

$$G = \frac{B_1 I + C_1}{A_2 I^2 + B_2 I + C_2}, \qquad (25)$$

$$\begin{aligned} F = F_\alpha + g(&\xi_{12}F_{v_1} + \xi_{23}F_{v_2} + \xi_{13}F_{v_3} + \xi_{21}F_{v_1^\dagger} \\ &+ \xi_{32}F_{v_2^\dagger} + \xi_{31}F_{v_3^\dagger} + \xi_{11}F_{z_1} + \xi_{33}F_{z_3}). \qquad (26) \end{aligned}$$

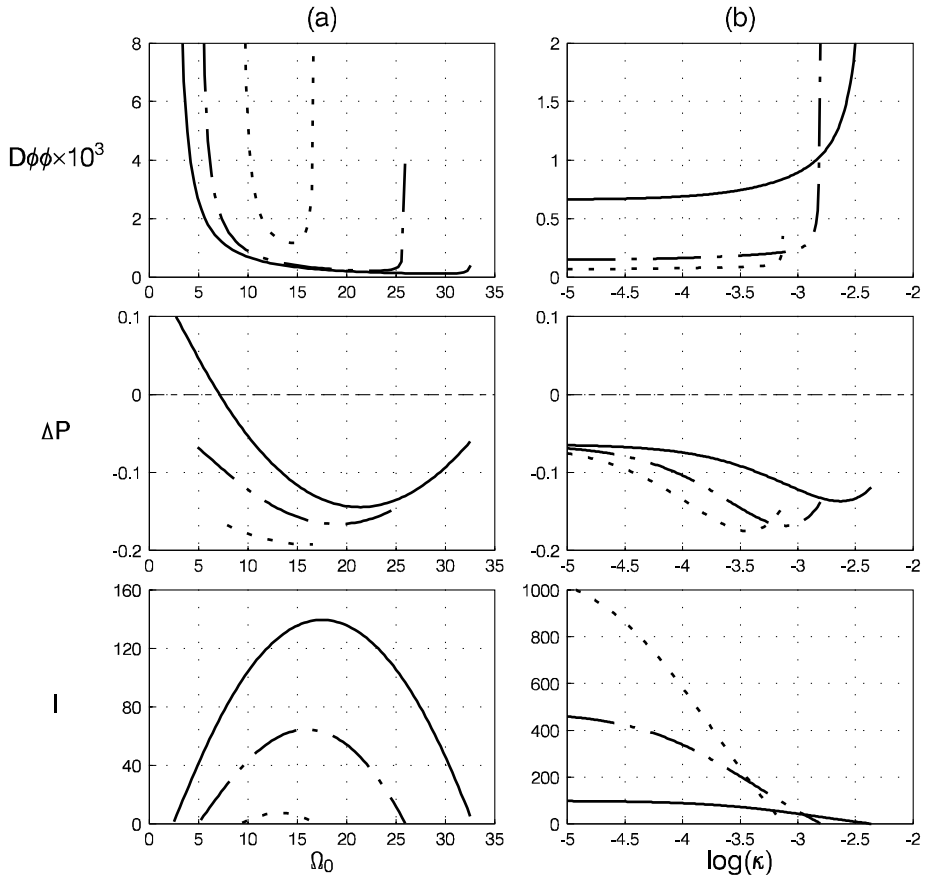

Fig. 2. For the V inversionless laser, linewidth $D_{\phi\phi}$ (together with the population difference ΔP, the laser intensity I) (a) *versus* Rabi frequency Ω_0 for $C = 1000$, $\bar{\gamma}_1 = 0.2$ (solid), 0.6 (dotted-dashed) and 1.0 (dotted); (b) *versus* cavity loss rate κ for $\bar{\gamma}_1 = 0.6$ and $\Omega_0 = 10$ (solid), 20 (dotted-dashed) and 30 (dotted). Other parameters are $\Lambda = 1.0$, $\gamma_2 = 4.0$.

The threshold condition ($G(0) = C_1/C_2 > \kappa$) is satisfied when

$$\left(\frac{B_3 - \sqrt{B_3^2 - 4q_3C_3}}{2q_3}\right)^{1/2} < \Omega_0 < \left(\frac{B_3 + \sqrt{B_3^2 - 4q_3C_3}}{2q_3}\right)^{1/2}. \quad (27)$$

The laser intensity $I = g^2\bar{n} = g^2\alpha^\dagger\alpha$ and the parameters in equations (25, 27) are presented in Appendix F. Note that the driving field Rabi frequency is limited to an upper limit $\Omega_0^{\max}$. If the Rabi frequency exceeds such a value, the driving field brings about such a strong saturation effect that the laser gain G is suppressed below the cavity loss rate κ. In the resonant case, α is assumed to be real without loss of generality. The parameters associated with the laser linewidth are

$$\begin{aligned}
\beta_1 &= \xi_{23} - \xi_{32} = (I + \gamma_{13}\gamma_{23})/U,\\
\beta_2 &= \xi_{12} - \xi_{21} = g\alpha\Omega_0/U,\\
\beta_3 &= \xi_{13} - \xi_{31} = \gamma_{23}\Omega_0/U,\\
U &= \gamma_{12}\gamma_{23}\gamma_{13} + \gamma_{12}I + \gamma_{23}I_0.
\end{aligned} \quad (28)$$

Above threshold, the linewidth takes the form

$$D_{\phi\phi} = \frac{g^4N}{2I}\sum_{i\le j;i,j=1}^{3}\beta_i\beta_j(\delta_{ij} + 2\delta_{i+1,j} + 2\delta_{i+2,j}) \times (\langle D_{x_i^\dagger x_j}\rangle - \langle D_{x_i x_j}\rangle), \quad (29)$$

where $x_1 = v_{21}$, $x_2 = v_{23}$, $x_3 = v_{31}$, $x_1^\dagger = v_{12}$, $x_2^\dagger = v_{32}$, $x_3^\dagger = v_{13}$. Atomic polarizations v_{ij} ($i \neq j$) and populations v_{ii}, which appear in equation (29), are presented in Appendix G. In the following calculation a nonzero constant γ_0 is chosen as the unit of the pump rates, decay rates and Rabi frequencies. Thus the linewidth $D_{\phi\phi}$ is in unit of g^4N/γ_0^3 and the laser intensity I is in unit of γ_0^2.

The threshold behavior is shown in Figure 2, where the linewidth $D_{\phi\phi}$ (together with the population difference $\Delta P = v_{11} - (v_{22} + v_{33})/2$ and the laser intensity I) is plotted (a) as function of the driving field Rabi frequency Ω_0 and (b) as function of the cavity loss rate κ. For the present case, the populations in the dressed state basis are associated with those in the bare state basis by the relations $R_{11} = v_{11}$ and $R_{22} = R_{33} = (v_{22} + v_{33})/2$. Thus we have $\Delta P = R_{11} - R_{22} (= R_{11} - R_{33})$. If $\Delta P < 0$ the system operates without inversion in the dressed state basis, and *vice versa*. It is well known that the linewidth depends on how far above threshold the system operates. Near above threshold, the laser intensity I is small and the linewidth $D_{\phi\phi}$ is substantially large. Well above threshold,

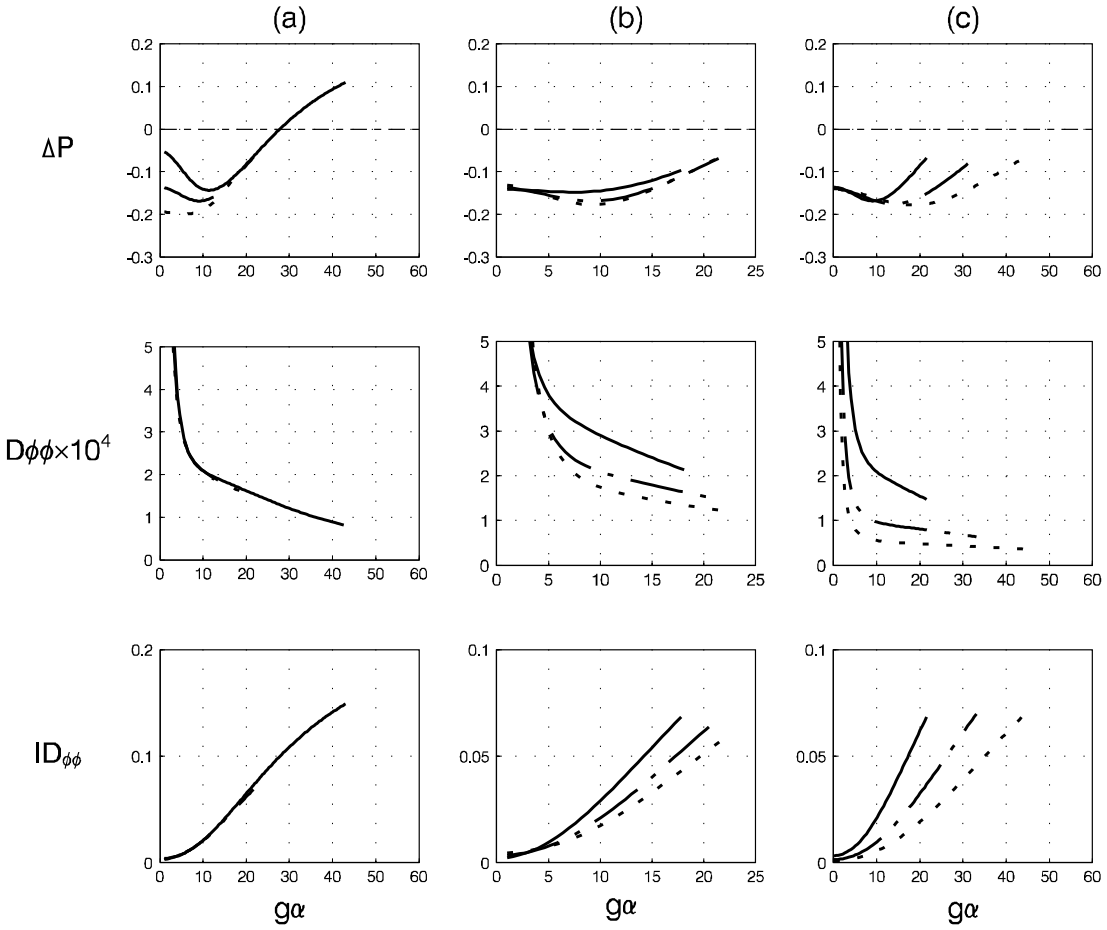

Fig. 3. For the V inversionless laser, population difference ΔP, Linewidth $D_{\phi\phi}$ and $ID_{\phi\phi}$ *versus* Rabi frequency $g\alpha$ (a) for $\Lambda = 1.0$, $\gamma_2 = 4$, $\Omega_0 = 20$, and $\bar{\gamma}_1 = 0.2$ (solid), 0.6 (dotted-dashed) and 1.0 (dotted); (b) for $\Lambda = 1.0$, $\bar{\gamma}_1 = 0.6$, $\Omega_0 = 20$, and $\gamma_2 = 2.0$ (solid), 4.0 (dotted-dashed) and 6.0 (dotted); (c) for $\Lambda = 1.0$, $\bar{\gamma}_1 = 0.6$, $\gamma_2 = 4.0$ and $\Omega_0 = 20$ (solid), 30 (dotted-dashed) and 40 (dotted).

the laser intensity I is greatly increased and the linewidth $D_{\phi\phi}$ is enormously reduced. Figure 2 exactly shows is exactly such a case. Note that there are two threshold values for the driving field Rabi frequency Ω_0 (Fig. 2a, also shown in Eq. (27)) where the linewidth $D_{\phi\phi}$ becomes very large. On the other hand, the smaller the cavity loss rate κ, the smaller the linewidth $D_{\phi\phi}$ (Fig. 2b).

Now we analyze the saturation effect of the laser intensity. In our calculation, we introduce the quantity $ID_{\phi\phi}$ (in unit of g^4N/γ_0). If this quantity is a constant as the laser intensity rises, it can be said that the linewidth has a $1/I$ decrease. For TLL, for example, the quantity $ID_{\phi\phi}$ approaches a constant and thus the linewidth exhibits the usual $1/I$ decrease. If, for other multilevel systems, this quantity increases with increasing I, the decrease in the linewidth is slower than $1/I$, and vice versa. For convenience we plot $D_{\phi\phi}$, $ID_{\phi\phi}$, and etc. *versus* the laser Rabi frequency $g\alpha$ instead of the laser intensity I.

For the inversionless laser, we plot in Figure 3 the population difference ΔP, the linewidth $D_{\phi\phi}$ and the quantity $ID_{\phi\phi}$ *versus* $g\alpha$ for various parameters. It is seen that the linewidth has the following two features. (i) The linewidth does not drop faster than $1/I$. When the intensity I is not too large, $ID_{\phi\phi}$ approaches a constant and thus the linewidth has the usual $1/I$ decay. For large laser intensity I, however, the decrease in $D_{\phi\phi}$ becomes slow and $ID_{\phi\phi}$ increases with increasing $g\alpha$. It is clear that the linewidth has a slower decay than $1/I$. (ii) The linewidth is insensitive to the transition from noninversion to inversion. As is shown by the solid lines in Figure 3a, although the system transits from noninversion to inversion as the intensity rises, the linewidth remains decreasing. In other words, the absence of inversion is not necessary for linewidth narrowing. This is in agreement with the result obtained from the linear analysis.

For the Raman laser, similarly, the decrease in the linewidth is not faster than $1/I$, as shown in Figure 4. However, a somewhat surprising result appears. The linewidth $D_{\phi\phi}$ itself increases with increasing $g\alpha$ in the range of the moderate Rabi frequency $g\alpha$. So far it has widely been held that the linewidth decreases with increasing laser intensity [2–7]. For the first time, it is shown that for the V Raman laser, increasing the laser intensity leads to linewidth broadening.

Comparing the V system with TLL, one can get an idea of the above saturation effects. For TLL, the population in the upper lasing level monotonously decreases as the laser intensity rises and the spontaneous emission itself becomes weak. Hence the linewidth has the usual $1/I$ dependence [2–4]. The case differs for the V system where a strong driving field is required to overcome the threshold. At least, compared with TLL, the population

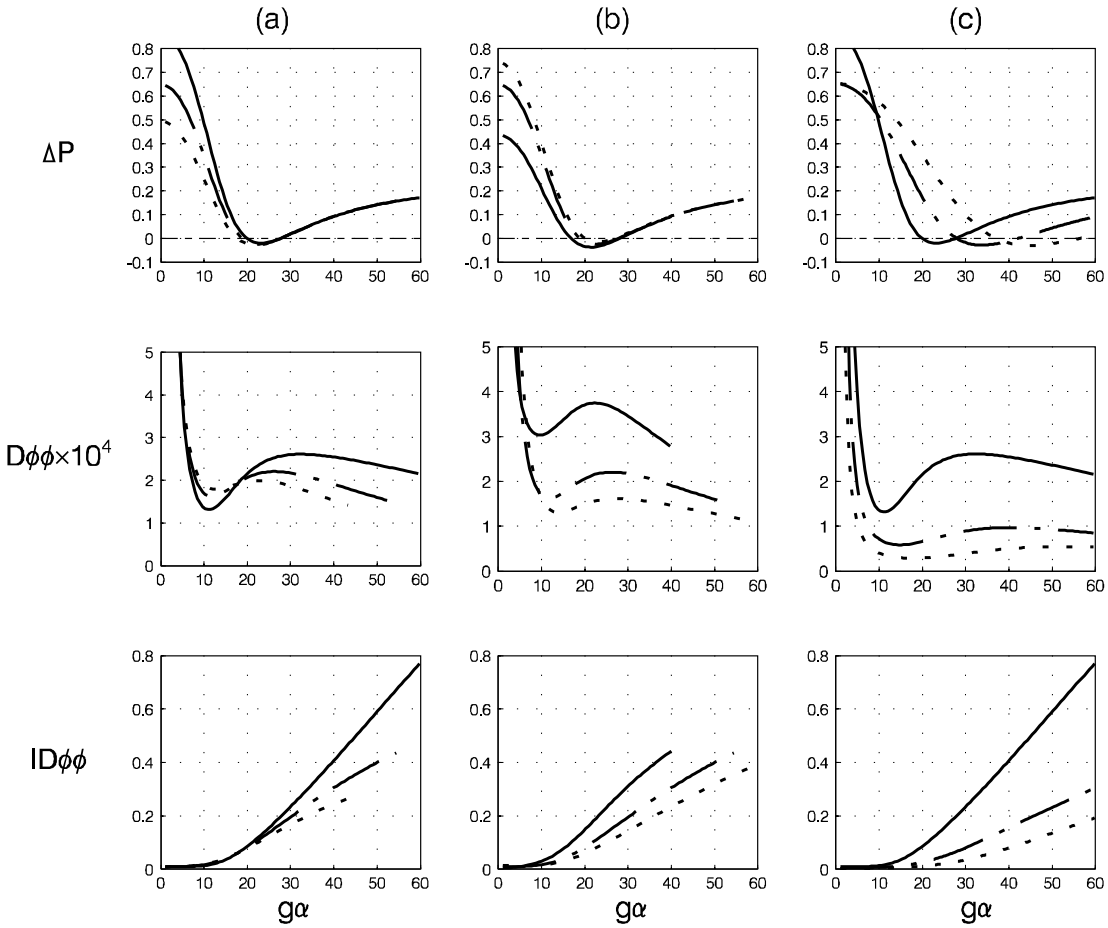

Fig. 4. For the V Raman laser, population difference ΔP, linewidth $D_{\phi\phi}$ and $ID_{\phi\phi}$ *versus* Rabi frequency $g\alpha$ (a) for $\Omega_0 = 20$, $\gamma_3 = 4.0$, and $\bar{\gamma}_1 = 0.2$ (solid), 0.6 (dotted-dashed) and 1.0 (dotted); (b) for $\Omega_0 = 20$, $\bar{\gamma}_1 = 0.6$, and $\gamma_3 = 2.0$ (solid), 4.0 (dotted-dashed) and 6.0 (dotted); (c) for $\gamma_3 = 4.0$, $\bar{\gamma}_1 = 0.6$, and $\Omega_0 = 20$ (solid), 30 (dotted-dashed) and 40 (dotted). The decay rate γ_2 has been neglected.

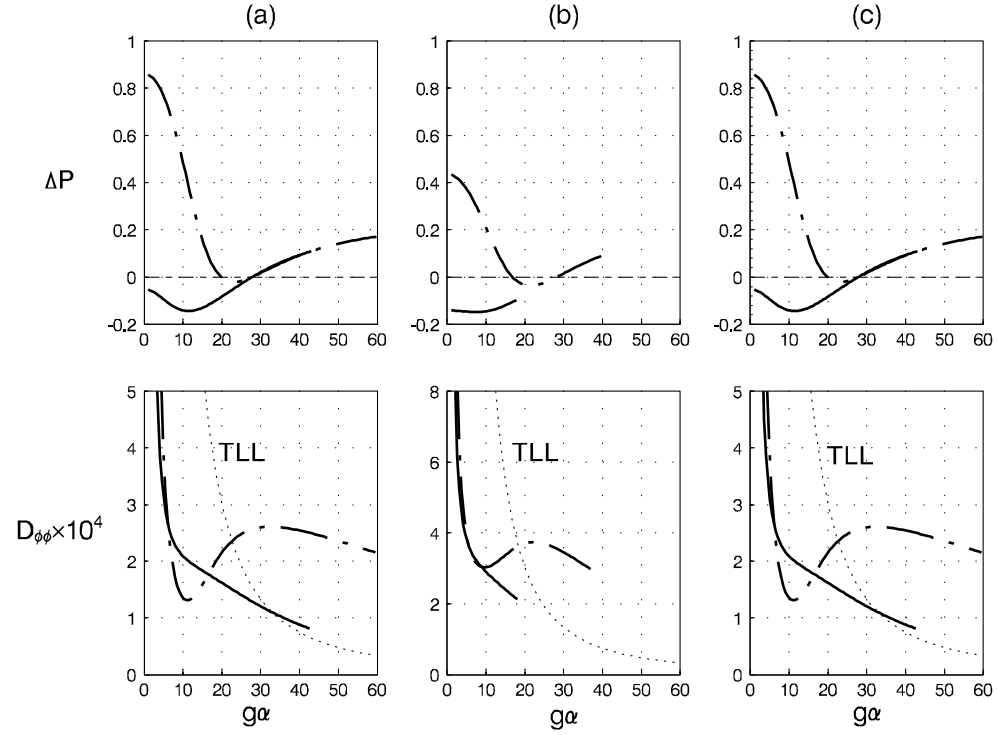

Fig. 5. Comparison between V inversionless (solid line) and Raman (dotted-dashed line) lasers and TLL (thin dashed line with a token "TLL"). The parameters for inversionless and Raman laser are the same as for the solid lines in Figures 3 and 4, respectively. For TLL, the parameters are chosen as $\Lambda = 4.0$, $\gamma_1 = 0.2$, and the population difference is not plotted since it is always positive.

in the upper lasing level has a slower decrease. Even the population does not decrease monotonously but increase in a certain range of intensity. In fact, as shown in Figures 3 and 4, the population difference also displays such a feature. Since the spontaneous emission is responsible for the laser linewidth, one expects that the linewidth of the V system does not decrease faster than $1/I$ and even increases a little in a certain regime of the laser intensity. In Figure 5 we show the comparison between the V lasers and TLL. For TLL, atoms are pumped from lower to upper lasing level with a rate 2Λ (through an auxiliary level from which atoms decay fast to the upper lasing level) and decay spontaneously from upper to lower level with a rate 2γ. Note that TLL operates well above threshold, $\Lambda = 20\gamma$. Figure 5 verifies the above results from linear and nonlinear analyses. (i) When the laser intensity is not too strong, the linewidths of the V lasers are narrower than that of TLL. As has already been pointed out in the above linear analysis, this is mainly due to the Autler-Townes splitting. (ii) When the laser intensity is strong, the linewidths of the V inversionless and Raman lasers may be larger than that of TLL. It is clear that this arises from the saturation effect of the laser field intensity. In addition, this result also supports the conclusion that the absence of population inversion is not really necessary for the linewidth reduction.

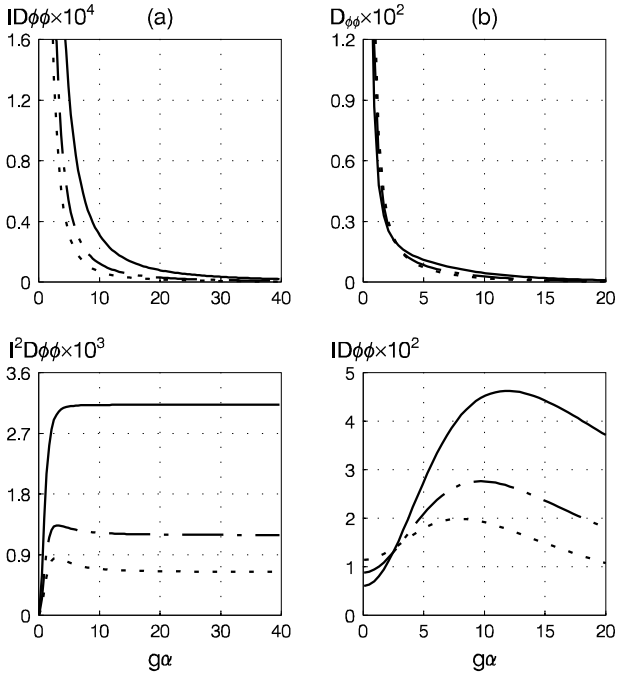

Fig. 6. For the Λ inversionless laser, (a) $ID_{\phi\phi}$ and $I^2D_{\phi\phi}$ *versus* $g\alpha$ for $\Omega_0 = 0.1$ ($\Omega_0 \ll \gamma_j$); (b) $D_{\phi\phi}$ and $ID_{\phi\phi}$ *versus* $g\alpha$ for $\Omega_0 = 10$ ($\Omega_0 \gg \gamma_j$). Other parameters: $\Lambda = 1.0$, $\bar{\gamma}_2 = 0.2$, and $\gamma_1 = 1.0$ (solid), 2.0 (dotted-dashed) and 3.0 (dotted).

5 Comparison between V and Λ lasers

It is interesting to compare the V lasers (Fig. 1a) with the Λ lasers (Fig. 1b). For the latter, similarly, a unified model is used to describe both an inversionless laser and a Raman laser. The parameters, which are labelled in Figure 1b, have the same meanings as in the V system. When $\Lambda = 0$ and $\gamma_3 \neq 0$, the model is the Raman scheme studied by Ritsch *et al.* [7] who showed that for the optimum conditions, the linewidth displays a fast $1/I^3$ decrease. When $\Lambda \neq 0$ and $\gamma_3 = 0$, the model is identical to the scheme studied by Imamaglu *et al.* [8,17]. However, how the linewidth depends on the laser intensity has not been given so far. Here it will be shown that for the optimum conditions, the linewidth decreases with $1/I^2$. On the other hand, for both inversionless and Raman lasers, it is possible that the linewidth decreases more slowly than $1/I$ in the strong driving limit.

Now the numerical results are presented in Figure 6 for the Λ inversionless laser. In the weak driving limit ($\Omega_0 \ll \gamma_j; j = 1{-}3$), curves $ID_{\phi\phi}$ (in unit of g^4N/γ_0) and $I^2D_{\phi\phi}$ (in unit of $g^4N\gamma_0$) *versus* $g\alpha$ are shown in Figure 6a. Note that the new quantity $I^2D_{\phi\phi}$ is used. In what follows the quantity $I^3D_{\phi\phi}$ (in unit of $g^4N\gamma_0^3$) will be used for the Raman laser. Generally speaking, if $I^mD_{\phi\phi}$ (in unit of $g^4N\gamma_0^{2m-3}$, m is the positive integer) remains unchanged as the intensity I rises, the linewidth decreases with $1/I^m$. It is seen from Figure 6a that for the optimum conditions ($\Omega_0 \ll \gamma_j \ll g\alpha$), the linewidth exhibits a fast $1/I^2$ decay. In the strong driving limit ($\Omega_0 \gg \gamma_j$), on the other hand, curves $D_{\phi\phi}$ and $ID_{\phi\phi}$ *versus* $g\alpha$ are plotted in Figure 6b. As the laser intensity rises, $ID_{\phi\phi}$ first changes very slowly, then increases and finally decreases. That is to say by varying the laser intensity we thus switch from the approximate $1/I$ decay, through the slower decay than $1/I$, to the faster decay than $1/I$. Unlike the V system where $ID_{\phi\phi}$ keeps increasing, $ID_{\phi\phi}$ of the Λ inversionless laser has its maximum value.

Next the results for the Λ Raman laser will be given. In Figure 7 we plot (a) $ID_{\phi\phi}$ and $I^3D_{\phi\phi}$ for the weak driving limit ($\Omega_0 \ll \gamma_2, \gamma_3$) and (b) $D_{\phi\phi}$ and $ID_{\phi\phi}$ for the strong driving limit ($\Omega_0 \gg \gamma_2, \gamma_3$). Clearly, $D_{\phi\phi}$ drops more quickly than $1/I$ in the weak driving limit. Well above threshold, $I^3D_{\phi\phi}$ approaches a constant and hence the linewidth $D_{\phi\phi}$ displays the fast $1/I^3$ dependence [7]. On the other hand, the Raman laser has the same features as the inversionless laser in the strong driving limit.

The distinct difference between the V and Λ lasers is that the linewidth of the Λ lasers may exhibit the faster decay than $1/I$ but the linewidth of the V lasers cannot. The physical origin of the above difference can be traced back to the basic difference in coherence lifetime and/or the difference in populations in the excited levels between the two systems. For V system, the coherence between states $|1\rangle$ and $|3\rangle$ has lifetime shorter than the lifetime of the laser transition. The short lifetime coherence not only brings about more noise but also leads to the more strict threshold condition, while the case differs for Λ system. Let's first compare the two cases in the weak driving limit. For the Λ system (Fig. 1b), any small driving field Rabi frequency can, in principle, result in lasing action. As the

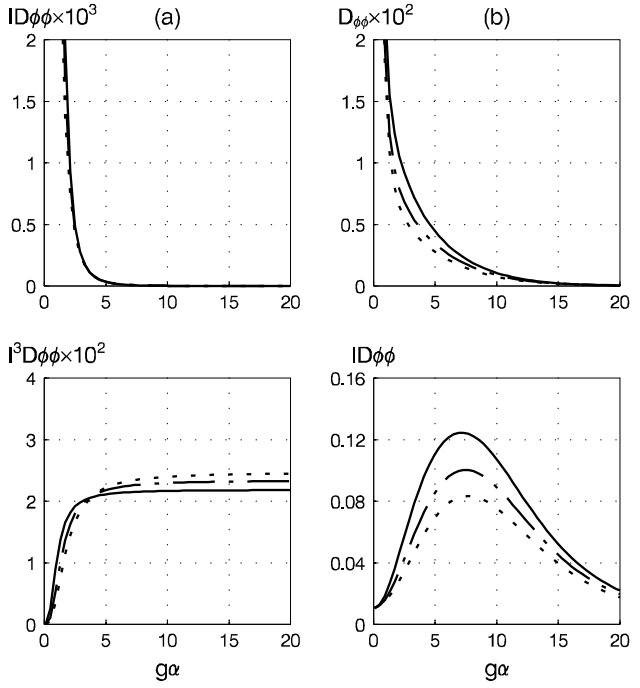

Fig. 7. For the Λ Raman laser, (a) $ID_{\phi\phi}$ and $I^3D_{\phi\phi}$ of *versus* $g\alpha$ for $\Omega_0 = 0.1$ ($\Omega_0 \ll \gamma_2, \gamma_3$); (b) $D_{\phi\phi}$ and $ID_{\phi\phi}$ of *versus* $g\alpha$ for $\Omega_0 = 10$ ($\Omega_0 \gg \gamma_2, \gamma_3$). Other parameters: $\gamma_3 = 2.0$, and $\bar{\gamma}_2 = 0.4$ (solid), 0.6 (dotted-dashed) and 0.8 (dotted). The decay rate γ_1 has been ignored.

laser intensity rises, more population stays in the auxiliary level $|1\rangle$ while less population is in the upper lasing level $|2\rangle$. Thus the spontaneous emission itself is very weak. It can be reasonably understood that the linewidth of the Λ system decreases more quickly than $1/I$ in the weak driving limit. For the V system, however, the minimum value of the required driving field Rabi frequency must have at least the same order as the decay rates. That means that the optimum condition for linewidth reduction is impossible. Then, we compare the two cases in the strong driving limit. In the regime near above threshold, the linewidths of the V and Λ systems have the $1/I$ decay due to the Autler-Townes splitting. For the moderate intensity, the upper lasing level has a increasing population. In this case, the linewidth has a slower decay than $1/I$. When the laser intensity is large enough, the upper lasing level $|2\rangle$ of the Λ system has a reduced population while the upper lasing level $|1\rangle$ of the V system continues to have a large population. As a result, the linewidth of the Λ lasers has the faster decay than $1/I$ while the linewidth of the V lasers still has the slower decay than $1/I$.

6 Conclusion

In conclusion, we have presented a detailed analysis of the spectral linewidth of the V inversionless and Raman lasers. The main points are summarized as follows. (i) The effects of the atomic coherence and the Autler-Townes splitting on the linewidth have been examined by employing the linear perturbation analysis in terms of the dressed state basis. It has been shown that near above threshold, the V inversionless laser has a linewidth far below that of TLL. However, the linewidth narrowing is not due to the dressed coherence but due to the Autler-Townes splitting, though the dressed coherence is crucial to the laser gain. (ii) The saturation effects of the laser intensity on the linewidth have been explored by applying the nonlinear analysis in the bare state basis. It has been predicted that the linewidths of both inversionless and Raman lasers do not decrease faster than $1/I$. The linewidth follows the usual $1/I$ decay in the regime of small laser intensity but the much slower decay than $1/I$ in the regime of large laser intensity. Unexpectedly, the linewidth of the V Raman laser does not decrease but appreciably increases with increasing laser intensity in a certain region of intensity. Therefore, well above threshold (in the region of large intensity), the V inversionless and Raman lasers may have a larger linewidth than that of TLL, while the case is reversed near above threshold. (iii) A comparison has been made between the V lasers and the Λ lasers. New predictions have been obtained for the Λ inversionless and Raman lasers. In the weak driving limit, the linewidth of the Λ inversionless laser shows the faster decay than $1/I$. In particular, well above threshold, the linewidth of the Λ inversionless laser displays the fast $1/I^2$ decay. In the strong driving limit, on the other hand, the linewidths of the Λ inversionless and Raman lasers have the slower decrease than $1/I$ in the region of low intensity and the faster decay than $1/I$ in the region of high intensity.

This work is supported by the National Natural Science Foundation of China under Grant No. 69708001 and by Foundation for University Key Teacher by the Ministry of Education.

Appendix A

In this appendix the master equation (5) is transformed into the equivalent form in the dressed state basis. In terms of the dressed-state operators $\tilde{\sigma}^j_{lk} = |\tilde{l}^j\rangle\langle\tilde{k}^j|$ ($\tilde{l}, \tilde{k} = \tilde{1}$–$\tilde{3}$), the bare state operators σ^j_{lk} ($l, k = 1$–3) are written as

$$\begin{aligned}
\sigma^j_{22} &= \cos^2\theta\tilde{\sigma}^j_{22} + \sin^2\theta\tilde{\sigma}^j_{33} + \tfrac{1}{2}\sin(2\theta)(\tilde{\sigma}^j_{23} + \tilde{\sigma}^j_{32}),\\
\sigma^j_{33} &= \sin^2\theta\tilde{\sigma}^j_{22} + \cos^2\theta\tilde{\sigma}^j_{33} - \tfrac{1}{2}\sin(2\theta)(\tilde{\sigma}^j_{23} + \tilde{\sigma}^j_{32}),\\
\sigma^j_{23} &= \tfrac{1}{2}\sin(2\theta)(-\tilde{\sigma}^j_{22} + \tilde{\sigma}^j_{33}) + \cos^2\theta\tilde{\sigma}^j_{23} - \sin^2\theta\tilde{\sigma}^j_{32},\\
\sigma^j_{12} &= \cos\theta\tilde{\sigma}^j_{12} + \sin\theta\tilde{\sigma}^j_{13},\\
\sigma^j_{13} &= -\sin\theta\tilde{\sigma}^j_{12} + \cos\theta\tilde{\sigma}^j_{13}.
\end{aligned} \tag{A.1}$$

The master equation (5) with (6) takes the form

$$\begin{aligned}
\dot{\tilde{\rho}} = &-\mathrm{i}[H_0, \tilde{\rho}] + \frac{1}{2}\kappa\mathcal{L}_{\mathrm{c}}\tilde{\rho}\\
&+ \sum_{j=1}^{N}\left(\gamma^j_1 L^j_{12}\tilde{\rho} + \gamma_2 L^j_{32}\tilde{\rho} + \Lambda L^j_{21}\tilde{\rho} + \gamma^j_3 L^j_{31}\tilde{\rho}\right),
\end{aligned} \tag{A.2}$$

$$H_0 = \Delta_c a^\dagger a + \sum_{j=1}^{N} \left[\Delta_1 \tilde{\sigma}_{11}^j + \lambda_2 \tilde{\sigma}_{22}^j + \lambda_3 \tilde{\sigma}_{33}^j + g\cos\theta(a^\dagger \tilde{\sigma}_{21}^j + \tilde{\sigma}_{12}^j a) + g\sin\theta(a^\dagger \tilde{\sigma}_{31}^j + \tilde{\sigma}_{13}^j a) \right], \tag{A.3}$$

$$L_{12}^j\tilde{\rho} = \cos^2\theta(2\tilde{\sigma}_{21}^j\tilde{\rho}\tilde{\sigma}_{12}^j - \tilde{\sigma}_{12}^j\tilde{\sigma}_{21}^j\tilde{\rho} - \tilde{\rho}\tilde{\sigma}_{12}^j\tilde{\sigma}_{21}^j) + \sin^2\theta(2\tilde{\sigma}_{31}^j\tilde{\rho}\tilde{\sigma}_{13}^j - \tilde{\sigma}_{13}^j\tilde{\sigma}_{31}^j\tilde{\rho} - \tilde{\rho}\tilde{\sigma}_{13}^j\tilde{\sigma}_{31}^j) + \sin(2\theta)(\tilde{\sigma}_{21}^j\tilde{\rho}\tilde{\sigma}_{13}^j + \tilde{\sigma}_{31}^j\tilde{\rho}\tilde{\sigma}_{12}^j) \tag{A.4}$$

$$\begin{aligned}
L_{32}^j\tilde{\rho} = {} & \cos^4\theta(2\tilde{\sigma}_{23}^j\tilde{\rho}\tilde{\sigma}_{32}^j - \tilde{\sigma}_{32}^j\tilde{\sigma}_{23}^j\tilde{\rho} - \tilde{\rho}\tilde{\sigma}_{32}^j\tilde{\sigma}_{23}^j) + \sin^4\theta(2\tilde{\sigma}_{32}^j\tilde{\rho}\tilde{\sigma}_{23}^j - \tilde{\sigma}_{23}^j\tilde{\sigma}_{32}^j\tilde{\rho} - \tilde{\rho}\tilde{\sigma}_{23}^j\tilde{\sigma}_{32}^j) \\
& + \frac{1}{4}\sin^2(2\theta)(2\tilde{\sigma}_{22}^j\tilde{\rho}\tilde{\sigma}_{22}^j - \tilde{\sigma}_{22}^{j2}\tilde{\rho} - \tilde{\rho}\tilde{\sigma}_{22}^{j2}) + \frac{1}{4}\sin^2(2\theta)(2\tilde{\sigma}_{33}^j\tilde{\rho}\tilde{\sigma}_{33}^j - \tilde{\sigma}_{33}^{j2}\tilde{\rho} - \tilde{\rho}\tilde{\sigma}_{33}^{j2}) \\
& - \frac{1}{2}\sin(2\theta)\cos^2\theta(2\tilde{\sigma}_{22}^j\tilde{\rho}\tilde{\sigma}_{32}^j - \tilde{\sigma}_{32}^j\tilde{\sigma}_{22}^j\tilde{\rho} - \tilde{\rho}\tilde{\sigma}_{32}^j\tilde{\sigma}_{22}^j) - \frac{1}{2}\sin(2\theta)\cos^2\theta(2\tilde{\sigma}_{23}^j\tilde{\rho}\tilde{\sigma}_{22}^j - \tilde{\sigma}_{22}^j\tilde{\sigma}_{23}^j\tilde{\rho} - \tilde{\rho}\tilde{\sigma}_{22}^j\tilde{\sigma}_{23}^j) \\
& - \frac{1}{2}\sin(2\theta)\sin^2\theta(2\tilde{\sigma}_{33}^j\tilde{\rho}\tilde{\sigma}_{23}^j - \tilde{\sigma}_{23}^j\tilde{\sigma}_{33}^j\tilde{\rho} - \tilde{\rho}\tilde{\sigma}_{23}^j\tilde{\sigma}_{33}^j) - \frac{1}{2}\sin(2\theta)\sin^2\theta(2\tilde{\sigma}_{32}^j\tilde{\rho}\tilde{\sigma}_{33}^j - \tilde{\sigma}_{33}^j\tilde{\sigma}_{32}^j\tilde{\rho} - \tilde{\rho}\tilde{\sigma}_{33}^j\tilde{\sigma}_{32}^j) \\
& - \frac{1}{4}\sin^2(2\theta)(2\tilde{\sigma}_{22}^j\tilde{\rho}\tilde{\sigma}_{33}^j + 2\tilde{\sigma}_{33}^j\tilde{\rho}\tilde{\sigma}_{22}^j) - \frac{1}{4}\sin^2(2\theta)(2\tilde{\sigma}_{23}^j\tilde{\rho}\tilde{\sigma}_{23}^j + 2\tilde{\sigma}_{32}^j\tilde{\rho}\tilde{\sigma}_{32}^j) \\
& + \frac{1}{2}\sin(2\theta)\sin^2\theta(2\tilde{\sigma}_{22}^j\tilde{\rho}\tilde{\sigma}_{23}^j + 2\tilde{\sigma}_{32}^j\tilde{\rho}\tilde{\sigma}_{22}^j) + \frac{1}{2}\sin(2\theta)\cos^2\theta(2\tilde{\sigma}_{33}^j\tilde{\rho}\tilde{\sigma}_{32}^j + 2\tilde{\sigma}_{23}^j\tilde{\rho}\tilde{\sigma}_{33}^j)
\end{aligned} \tag{A.5}$$

$$\begin{aligned}
L_{21}^j\tilde{\rho} = {} & \cos^2\theta(2\tilde{\sigma}_{12}^j\tilde{\rho}\tilde{\sigma}_{21}^j - \tilde{\sigma}_{21}^j\tilde{\sigma}_{12}^j\tilde{\rho} - \tilde{\rho}\tilde{\sigma}_{21}^j\tilde{\sigma}_{12}^j) + \sin^2\theta(2\tilde{\sigma}_{13}^j\tilde{\rho}\tilde{\sigma}_{31}^j - \tilde{\sigma}_{31}^j\tilde{\sigma}_{13}^j\tilde{\rho} - \tilde{\rho}\tilde{\sigma}_{31}^j\tilde{\sigma}_{13}^j) \\
& + \frac{1}{2}\sin(2\theta)(2\tilde{\sigma}_{12}^j\tilde{\rho}\tilde{\sigma}_{31}^j - \tilde{\sigma}_{31}^j\tilde{\sigma}_{12}^j\tilde{\rho} - \tilde{\rho}\tilde{\sigma}_{31}^j\tilde{\sigma}_{12}^j) + \frac{1}{2}\sin(2\theta)(2\tilde{\sigma}_{13}^j\tilde{\rho}\tilde{\sigma}_{21}^j - \tilde{\sigma}_{21}^j\tilde{\sigma}_{13}^j\tilde{\rho} - \tilde{\rho}\tilde{\sigma}_{21}^j\tilde{\sigma}_{13}^j)
\end{aligned} \tag{A.6}$$

$$\begin{aligned}
L_{31}\tilde{\rho} = {} & \sin^2\theta(2\tilde{\sigma}_{12}\tilde{\rho}\tilde{\sigma}_{21} - \tilde{\sigma}_{21}\tilde{\sigma}_{12}\tilde{\rho} - \tilde{\rho}\tilde{\sigma}_{21}\tilde{\sigma}_{12}) + \cos^2\theta(2\tilde{\sigma}_{13}\tilde{\rho}\tilde{\sigma}_{31} - \tilde{\sigma}_{31}\tilde{\sigma}_{13}\tilde{\rho} - \tilde{\rho}\tilde{\sigma}_{31}\tilde{\sigma}_{13}) \\
& - \frac{1}{2}\sin(2\theta)(2\tilde{\sigma}_{12}\tilde{\rho}\tilde{\sigma}_{31} - \tilde{\sigma}_{31}\tilde{\sigma}_{12}\tilde{\rho} - \tilde{\rho}\tilde{\sigma}_{31}\tilde{\sigma}_{12}) - \frac{1}{2}\sin(2\theta)(2\tilde{\sigma}_{13}\tilde{\rho}\tilde{\sigma}_{21} - \tilde{\sigma}_{21}\tilde{\sigma}_{13}\tilde{\rho} - \tilde{\rho}\tilde{\sigma}_{21}\tilde{\sigma}_{13})
\end{aligned} \tag{A.7}$$

---

where

see equations (A.3–A.7) above.

Using the above operator equations (A.2–A.7) we can easily write the Langevin equations (8).

Appendix B

This appendix presents the parameters in equation (8),

$$\begin{aligned}
&g_1 = g\cos\theta, && g_2 = g\sin\theta, \\
&\Lambda_1 = \Lambda\cos^2\theta, && \Lambda_2 = \Lambda\sin^2\theta, \\
&\Gamma_1 = \gamma_1\cos^2\theta, && \Gamma_2 = \gamma_1\sin^2\theta, \\
&\Gamma_{32} = \gamma_2\cos^4\theta, && \Gamma_{23} = \gamma_2\sin^4\theta, \\
&\Lambda_c = \sqrt{\Lambda_1\Lambda_2}, && \gamma_c = \tfrac{1}{2}\gamma_2\sin(2\theta), \\
&\Gamma_c = \tfrac{1}{4}\gamma_2\sin(4\theta), && \Gamma_p = \sqrt{\Gamma_{23}\Gamma_{32}}, \\
&\Gamma_q = \sqrt{\Gamma_1\Gamma_2}, && \tilde{\Delta}_1 = \Delta_1 - \lambda_2, \\
&\tilde{\Delta}_2 = \Delta_1 - \lambda_3, && \tilde{\Delta}_3 = \tilde{\Delta}_2 - \tilde{\Delta}_1, \\
&\tilde{\gamma}_{21} = \gamma_1 + \Lambda_1 + \Gamma_{23} + \Gamma_p, && \tilde{\gamma}_{31} = \gamma_1 + \Lambda_2 + \Gamma_{32} + \Gamma_p, \\
&\tilde{\gamma}_{32} = \Lambda + \Gamma_{23} + \Gamma_{32} + 4\Gamma_p.
\end{aligned}$$

Appendix C

This appendix shows the steady state populations, polarization and parameters in equation (20) for general off-resonance. The populations R_{ii} and polarization R_{23} read

$$\begin{aligned}
&R_{ii} = Q_i/Q, \qquad i = 1\text{–}3, \\
&R_{23} = w\left(2\Gamma_q R_{11} + w_1 R_{22} + w_2 R_{33}\right),
\end{aligned} \tag{C.1}$$

where

$$\begin{aligned}
Q &= u_1v_2 + u_2v_3 + u_3v_1 - u_1v_3 - u_2v_1 - u_3v_2, \\
Q_1 &= u_2v_3 - u_3v_2, \\
Q_2 &= u_3v_1 - u_1v_3, \\
Q_3 &= u_1v_2 - u_2v_1.
\end{aligned} \tag{C.2}$$

Here the parameters are

$$\begin{aligned}
&w_1 = 2\gamma_c - \Gamma_c - \Lambda_c, && w_2 = 2\gamma_c + \Gamma_c - \Lambda_c, \\
&w = (\chi_{32} - 2\Gamma_p)/(|\chi_{31}|^2 - 4\Gamma_p^2), && u_0 = -(\Lambda_c + \Gamma_c), \\
&u_1 = 2\Gamma_1 + 4u_0 w\Gamma_q, && u_2 = -2(\Lambda_1 + \Gamma_{23}) \\
&u_3 = 2\Gamma_{32} + 2u_0 w w_2, && \quad + 2u_0 w w_1, \\
&v_1 = 2\Gamma_2 + 4v_0 w\Gamma_q, && v_0 = -(\Lambda_c - \Gamma_c), \\
&v_3 = -2(\Lambda_2 + \Gamma_{32}) + 2v_0 w w_1, && v_2 = 2\Gamma_{23} + 2v_0 w w_2,
\end{aligned} \tag{C.3}$$

with $\chi_{31} = \tilde{\gamma}_{31} + \mathrm{i}\tilde{\Delta}_1$, $\chi_{32} = \tilde{\gamma}_{32} + \mathrm{i}\tilde{\Delta}_3$.

The parameters in equations (20) read:

$$\begin{aligned}
a_1 &= \mathrm{Re}\,\frac{g_1^2\chi_{31}^2 - g_1g_2v}{g^2(\chi_{21}\chi_{31} - v^2)}, \\
a_2 &= \mathrm{Re}\,\frac{g_2^2\chi_{21} - g_1g_2v}{g^2(\chi_{21}\chi_{31} - v^2)}, \\
b_1 &= \frac{g_2^2v - g_1g_2\chi_{31}}{g^2(\chi_{21}\chi_{31} - v^2)}, \\
b_2 &= \frac{g_1^2v - g_1g_2\chi_{21}}{g^2(\chi_{21}\chi_{31} - v^2)},
\end{aligned} \tag{C.4}$$

where $\chi_{21} = \gamma_{21} + \mathrm{i}\tilde{\Delta}_1$, $v = (\Lambda - \gamma_2)\sin\theta\cos\theta$.

Appendix D

This appendix lists the parameters in the linewidth formula (21),

$$
\begin{aligned}
c_1 &= \frac{2}{g^2}\left|\frac{g_1\chi_{31}-g_2 v}{\chi_{21}\chi_{31}-v^2}\right|^2,\\
c_2 &= \frac{2}{g^2}\left|\frac{g_2\chi_{21}-g_1 v}{\chi_{21}\chi_{31}-v^2}\right|^2,\\
c_3 &= \frac{-4}{g^2}\,\mathrm{Re}\left[\frac{(g_1\chi_{31}^*-g_2 v)(g_2\chi_{21}-g_1 v)}{(\chi_{21}^*\chi_{31}^*-v^2)(\chi_{21}\chi_{31}-v^2)}\right].
\end{aligned}
\tag{D.1}
$$

Appendix E

Using the Einstein relations [2–4], we easily derive the diffusion coefficients from the Langevin equations (23),

$$
\begin{aligned}
2\langle D_{v_{21}v_{21}}\rangle &= 2g\alpha v_{21},\\
2\langle D_{v_{23}v_{23}}\rangle &= 2\Omega v_{23},\\
2\langle D_{v_{12}v_{21}}\rangle &= 2\Lambda(v_{11}+v_{22})+2\gamma_3 v_{33},\\
2\langle D_{v_{32}v_{23}}\rangle &= 2\Lambda v_{33}+2\gamma_3 v_{11},\\
2\langle D_{v_{13}v_{31}}\rangle &= 2\Lambda v_{22}+2\gamma_2 v_{11}+2\gamma_3(v_{11}+v_{33})\\
&\quad -g\alpha^\dagger v_{21}-g\alpha v_{12},\\
2\langle D_{v_{23}v21}\rangle &= g\alpha v_{23}+\Omega v_{21},\\
2\langle D_{v_{31}v_{23}}\rangle &= -g\alpha(v_{11}-v_{33})-\Omega v_{31},\\
2\langle D_{v_{31}v_{21}}\rangle &= g\alpha v_{31},\\
2\langle D_{v_{12}v_{23}}\rangle &= 2\Lambda v_{13}.
\end{aligned}
$$

Appendix F

The parameters in equations (25, 27) are given as follows,

$$
\begin{aligned}
B_1 &= 2g^2 N p_1,\\
B_2 &= (q_5-q_2-q_4)I_0+q_1\gamma_{12}+2q_2\gamma_{13}\gamma_{23},\\
C_1 &= 2g^2 N[(p_2+p_3\gamma_{13})I_0+p_1\gamma_{13}\gamma_{23}],\\
C_2 &= q_3 I_0^2+(q_1\gamma_{23}+q_3\gamma_{12}\gamma_{13})I_0+q_1\gamma_{12}\gamma_{23}\gamma_{13},\\
B_3 &= (q_1\gamma_{23}+q_3\gamma_{12}\gamma_{13})-2g^2 N(p_2+p_3\gamma_{13})/\kappa,\\
C_3 &= q_1\gamma_{12}\gamma_{23}\gamma_{13}-2g^2 N p_1\gamma_{13}\gamma_{23}/\kappa,
\end{aligned}
\tag{F.1}
$$

where

$$
\begin{aligned}
&q_1=(\gamma_1+\Lambda)(\gamma_2+\gamma_3),\ q_2=\gamma_2+\gamma_3,\\
&q_3=2\gamma_1+\gamma_3+\Lambda, \qquad q_4=\gamma_1+2\gamma_3-\Lambda,\\
&q_5=3\gamma_{13}, \qquad p_1=(\Lambda-\gamma_1)(\gamma_2+\gamma_3),\\
&p_2=\gamma_1(\gamma_2+\gamma_3), \qquad p_3=\Lambda+\gamma_3-\gamma_1,
\end{aligned}
\tag{F.2}
$$

By neglecting the noise in the equation (24), we obtain the laser intensity $I=g^2\bar{n}=g^2\alpha^\dagger\alpha$,

$$
I=\frac{-B+\sqrt{B^2-4A_2C}}{2A_2},
\tag{F.3}
$$

where $A_2=2q_2$, $B=B_2-B_1/\kappa$, $C=C_2-C_1/\kappa$

Appendix G

This appendix presents the atomic polarizations and populations in the steady state. The atomic polarizations are written in the form

$$
\begin{aligned}
v_{12} &= g\alpha[p_1 I+(p_2+p_3\gamma_{13})I_0+p_1\gamma_{13}\gamma_{23}]/W,\\
v_{23} &= -\Omega_0[p_2 I_0+(p_1-p_4\gamma_{13})I+p_2\gamma_{13}\gamma_{12}]/W,\\
v_{13} &= -g\alpha\Omega_0[p_4 I+p_3 I_0+(p_1\gamma_{23}-p_2\gamma_{12})]/W.
\end{aligned}
\tag{G.1}
$$

where $W=A_2I^2+B_2I+C_2$, $p_4=-\gamma_2-\gamma_3$. The atomic populations read

$$
\begin{aligned}
v_{11} &= \frac{1}{W}\left\{\begin{array}{l}(\gamma_2+\gamma_3)I^2+(\Lambda+\gamma_3)I_0^2\\ +(\gamma_{13}-\gamma_2-2\gamma_3)II_0\\ +[\gamma_{13}\gamma_{23}(\gamma_2+\gamma_3)+\Lambda\gamma_{12}(\gamma_2+\gamma_3)]I\\ +[(\Lambda+\gamma_3)\gamma_{13}\gamma_{12}+\Lambda\gamma_{23}(\gamma_2+\gamma_3)]I_0\\ +\Lambda(\gamma_2+\gamma_3)\gamma_{12}\gamma_{23}\gamma_{13}\end{array}\right\},\\
v_{22} &= \frac{1}{W}\left\{\begin{array}{l}(\gamma_2+\gamma_3)I^2+\gamma_1 I_0^2+(\gamma_{13}-\gamma_3)II_0\\ +[(\gamma_2+\gamma_3)\gamma_{13}\gamma_{23}+\gamma_1\gamma_{12}(\gamma_2+\gamma_3)]I\\ +\gamma_1[\gamma_{13}\gamma_{12}+\gamma_{23}(\gamma_2+\gamma_3)]I_0\\ +\gamma_1(\gamma_2+\gamma_3)\gamma_{12}\gamma_{23}\gamma_{13}\end{array}\right\},\\
v_{33} &= \frac{1}{W}[\gamma_1 I_0^2+(\Lambda+\gamma_{13}-\gamma_1)II_0+\gamma_1\gamma_{13}\gamma_{12}I_0].
\end{aligned}
\tag{G.2}
$$

References

1. A.L. Schawlow, C.H. Townes, Phys. Rev. **112**, 1940 (1958).
2. H. Haken, in *Laser Theory,* edited by S. Flugge, Encyclopedia of Physics Vol. XXV/2c (Springer-Verlag, Heidelberg, 1970).
3. M. Sargent III, M.O. Scully, W.E. Lamb Jr, *Laser Physics* (Addison-Wesley, Reading, Massachusetts, 1974).
4. W.H. Louisell, *Quantum Statistical Properties of Radiation* (Wiley, New York, 1973).
5. G.S. Agarwal, Phys. Rev. Lett. **67**, 980 (1991).
6. M. Fleischhauer, U. Rathe, M.O. Scully, Phys. Rev. A **50**, 1748 (1994).
7. H. Ritsch, M.A.M. Marte, P. Zoller, Europhys. Lett. **19**, 7 (1993); H. Ritsch, M.A.M. Marte, Phys. Rev. A **47**, 2354 (1993).
8. K.M. Gheri, D.F. Walls, Phys. Rev. Lett. **68**, 3428 (1992); Phys. Rev. A **45**, 6675 (1992).
9. A.S. Manka, C.H. Keitel, S.Y. Zhu, M. Fleischhauer, L.M. Narducci, M.O. Scully, Opt. Commun. **94**, 174 (1992).
10. C. Saavedra, J.C. Retamal, H. Keitel, Phys. Rev. A **55**, 3802 (1997).
11. K.J. Schernthanner, H. Ritsch, Phys. Rev. A **49**, 4126 (1994).

12. Y. Zhu, M. Xiao, Phys. Rev. A **48**, 3895 (1993).
13. X.M. Hu, J.S. Peng, Eur. Phys. J. D **5**, 291 (1999); Opt. Commun. **160**, 241 (1999); J. Phys. B **31**, 5393 (1998); J. Opt. B **1**, 598 (1999).
14. Y. Zhu, A.I. Rubiera, M. Xiao, Phys. Rev. A **53**, 1065 (1996).
15. S.E. Harris, Phys. Rev. Lett. **62**, 1033 (1989); A. Imamoglu, S.E. Harris, Opt. Lett. **14**, 1344 (1989); A. Imamoglu, Phys. Rev. A **40**, 2835 (1989).
16. M.O. Scully, S.Y. Zhu, A. Gavrielides, Phys. Rev. Lett. **62**, 2813 (1989).
17. A. Imamoglu, J.E. Field, S.E. Harris, Phys. Rev. Lett. **64**, 1154 (1991).
18. Y. Zhu, Phys. Rev. A **45**, R6149 (1992).
19. G.S. Agarwal, Phys. Rev. A **44**, R28 (1991); C.H. Keitel, O.A. Kocharovskaya, L.M. Narducci, M.O. Scully, S.Y. Zhu, H.M. Doss, Phys. Rev. A **48**, 3196 (1993)
20. J. Gao, C. Guo, X. Guo, G. Jin, P. Wang, J. Zhao, H. Zhang, Y. Jiang, D. Wang, D. Jiang, Opt. Commun. **93**, 323 (1992).
21. A. Nottelmann, C. Peters, W. Lange, Phys. Rev. Lett. **70**, 1783 (1993).
22. E.S. Fry, X. Li, D. Nikonov, G.G. Padmabandu, M.O. Scully, A.V. Smith, F.K. Tittel, C. Wang, S.R. Wilkinson, S.Y. Zhu, Phys. Rev. Lett. **70**, 3235 (1993).
23. W.E. van der Veer, R.J.J. van Diest, A. Donszelmann, H.B. van Linden van den Heuvell, Phys. Rev. Lett. **70**, 3243 (1993).
24. A.S. Zibrov, M.D. Lukin, D.E. Nikonov, L. Hollberg, M.O. Scully, V.L. Velichansky, H.G. Robinson, Phys. Rev. Lett. **75**, 1499 (1995).
25. G.G. Padmabandu, G.R. Welch, I.N. Shubin, E.S. Fry, D.E. Nikonov, M.D. Lukin, M.O. Scully, Phys. Rev. Lett. **76**, 2053 (1996).
26. S.H. Autler, C.H. Townes, Phys. Rev. **100**, 703 (1955).
27. B.R. Mollow, Phys. Rev. **188**, 1969 (1969); Phys. Rev. A **5**, 2217(1972).
28. L.M. Narducci, M.O. Scully, G.-L. Oppo, P. Ru, J.R. Tredicce, Phys. Rev. A **42** 1630 (1990).
29. S.Y. Zhu, M.O. Scully, Phys. Lett. A **201**, 85 (1995); S.Y. Zhu, L.M. Narducci, M.O. Scully, Phys. Rev. A **52**, 4791 (1995).
30. P.D. Drummond, C.W. Gardiner, J. Phys. A **13**, 2353 (1980).